LETTER

doi:10.1038/nature25787

The mechanism of eukaryotic CMG helicase activation

Max E. Douglas[1], Ferdos Abid Ali[2], Alessandro Costa[2] & John F. X. Diffley[1]

The initiation of eukaryotic DNA replication occurs in two discrete stages[1]: first, the minichromosome maintenance (MCM) complex assembles as a head-to-head double hexamer that encircles duplex replication origin DNA during G1 phase; then, 'firing factors' convert each double hexamer into two active Cdc45–MCM–GINS helicases (CMG) during S phase. This second stage requires separation of the two origin DNA strands and remodelling of the double hexamer so that each MCM hexamer encircles a single DNA strand. Here we show that the MCM complex, which hydrolyses ATP during double-hexamer formation[2,3], remains stably bound to ADP in the double hexamer. Firing factors trigger ADP release, and subsequent ATP binding promotes stable CMG assembly. CMG assembly is accompanied by initial DNA untwisting and separation of the double hexamer into two discrete but inactive CMG helicases. Mcm10, together with ATP hydrolysis, then triggers further DNA untwisting and helicase activation. After activation, the two CMG helicases translocate in an 'N terminus-first' direction, and in doing so pass each other within the origin; this requires that each helicase is bound entirely to single-stranded DNA. Our experiments elucidate the mechanism of eukaryotic replicative helicase activation, which we propose provides a fail-safe mechanism for bidirectional replisome establishment.

Previous studies have focused on the activities of CMG that is preassembled by co-overexpression of individual subunits[4,5]. Here we aimed to understand how CMG is assembled and activated during the initiation of DNA replication, using purified budding yeast proteins[6]. We first used a DNA-topology-based assay[7] (Fig. 1a) to study the unwinding of DNA by CMG. In the presence of topoisomerase I (Topo I), the DNA linking number of a covalently closed circular DNA molecule decreases by one for each helical turn that is untwisted, allowing changes in DNA unwinding to be inferred quantitatively from changes in DNA supercoiling. We loaded MCM onto a relaxed, circular plasmid in solution, phosphorylated MCM with Dbf4-dependent kinase (DDK), and incubated this with firing factors (defined as Clb5–Cdc28 (hereafter CDK), Cdc45, GINS complex (hereafter GINS), Sld2, Sld3, Sld7, Dpb11, DNA polymerase ε and Mcm10), replication protein A (RPA), and Topo I in the presence of ATP (Fig. 1b). After incubation, DNA was isolated and plasmid topology was examined by native agarose gel electrophoresis. A fraction of the relaxed plasmid DNA became supercoiled in a time-dependent manner (Fig. 1c), but not when DDK, CDK, Cdc45, GINS, Mcm10 or RPA were omitted (Fig. 1d). These results show that CMG assembled from the double hexamer can unwind DNA even when uncoupled from DNA synthesis, consistent with previous experiments[6,8]. Mcm10 is required for unwinding (Fig. 1d) but not for CMG formation[1,6]. Mcm10 supported extensive unwinding and DNA synthesis even when added after CMG assembly was finished (Extended Data Fig. 1a–d). Thus, Mcm10 activates CMG helicase in a distinct step after CMG assembly (Extended Data Fig. 1e).

The amount of supercoiling that occurs in the absence of RPA should reflect DNA untwisting that is constrained by the CMG (see Extended Data Fig. 2a). To assess this, we constructed a covalently closed, circular 616-base-pair (bp) radiolabelled DNA molecule, which allows us to quantify even small changes in topoisomer distribution relative to the relaxed ground state (α) (Extended Data Fig. 2b). CMG assembly and activation in the absence of RPA shifted a proportion of the four starting topoisomers ($\alpha+1$, α, $\alpha-1$, $\alpha-2$) to a new set of supercoils, $\alpha-3$, $\alpha-4$, $\alpha-5$ and $\alpha-6$ indicating that each circle had been unwound by 3–4 helical turns (Fig. 2a, lane 2). This is likely to be due to genuine

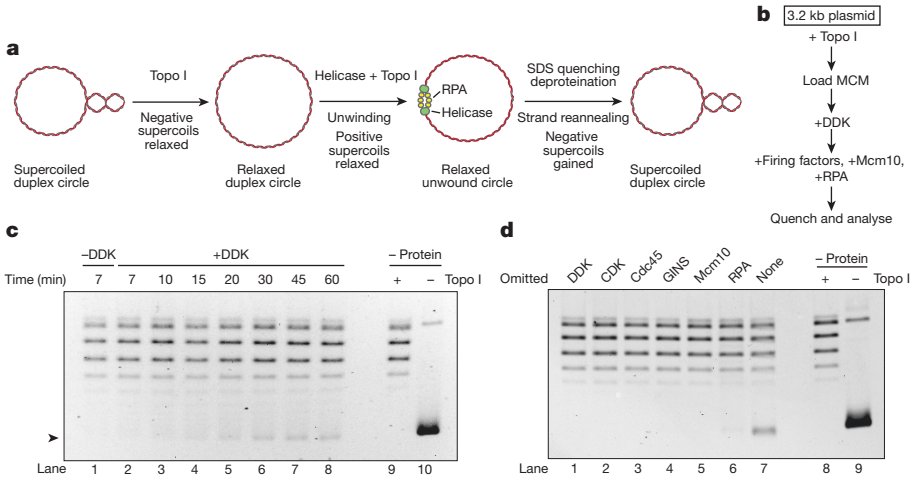

Figure 1 | Analysis of replicative helicase activation with a DNA unwinding assay. a, **b**, Outline of the assay. **c**, Time course of unwinding. Purified DNA products were separated on a native agarose gel and stained with ethidium bromide. No loading or firing factors were added to '−protein' reactions. Arrowhead indicates supercoiled plasmid DNA. **d**, As **c**, with omission of the indicated proteins. Reactions were quenched after 40 min.

[1]Chromosome Replication Laboratory, The Francis Crick Institute, 1 Midland Road, London NW1 1AT, UK. [2]Macromolecular Machines Laboratory, The Francis Crick Institute, 1 Midland Road, London NW1 1AT, UK.

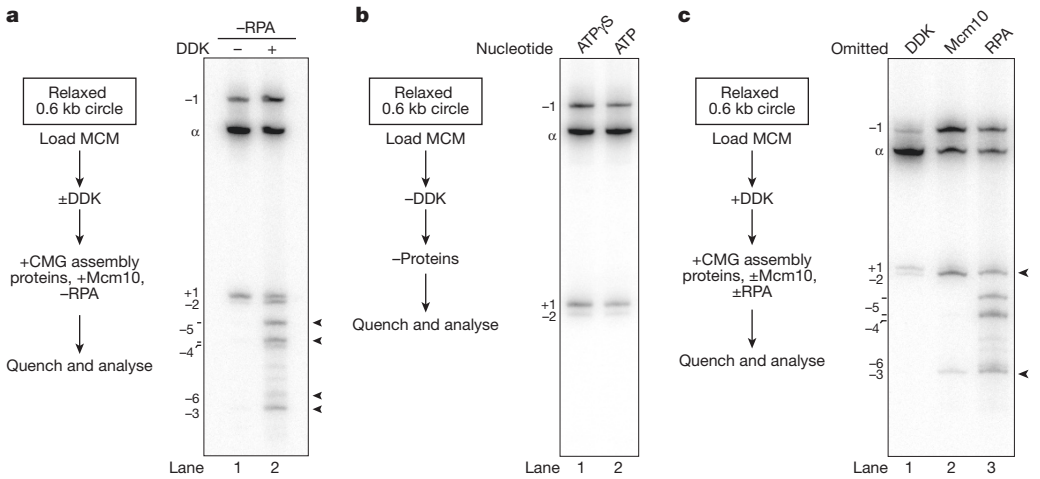

Figure 2 | Origin unwinding takes place in two steps. a, Active CMG was assembled on a radiolabelled 616-bp *ARS1* circle in the absence of RPA for 40 min and products were separated on a native bis-polyacrylamide gel. Arrowheads indicate topoisomers observed after CMG assembly and activation. **b**, As **a**, except all firing factors were omitted. MCM loading does not occur with ATPγS. **c**, As **a**, with omission of the indicated proteins. Arrowheads indicate topoisomers observed after CMG assembly without Mcm10.

unwinding, because thymine residues in DNA became reactive to potassium permanganate ($KMnO_4$) across a wide region (Extended Data Fig. 2c). Thus, each of the two activated CMG helicases constrains approximately 1.5–2 helical turns of unwound DNA.

On the basis of the kinked central channel at the interface between hexamers[9,10], it has been hypothesized that duplex DNA may be distorted by the double hexamer[10]. However, the topoisomer distribution was identical when circles were incubated with loading factors and Topo I in ATPγS (preventing double-hexamer assembly) or ATP (enabling double-hexamer assembly) (Fig. 2b), indicating that DNA in the double hexamer is not notably untwisted, consistent with recent cryo-electron microscopy (cryo-EM) structures of double hexamer with DNA[11,12]. By contrast, incubation of double hexamer with a full complement of firing factors in the absence of Mcm10 shifted a proportion of circles to more negatively supercoiled topoisomers (Fig. 2c, lane 2: $\alpha-2$ and $\alpha-3$). Supercoiling required MCM loading (Extended Data Fig. 2d) and all firing factors (Extended Data Fig. 2e), indicating that it takes place during CMG assembly. This shift in supercoiling

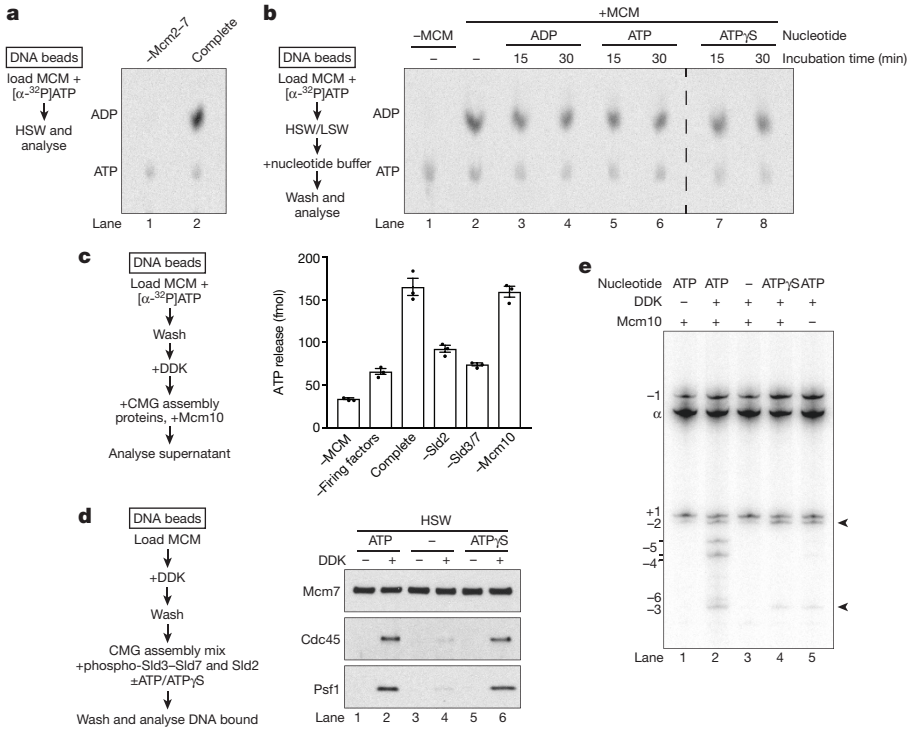

Figure 3 | CMG assembly and activation are coupled to ATP binding and hydrolysis. a, MCM-loading reactions containing [α-^{32}P]ATP were washed with high-salt buffer (buffer A + NaCl, HSW) and analysed by thin layer chromatography. **b**, As **a**, except washed reactions were incubated with nucleotide as indicated and washed again before analysis. LSW, low-salt buffer. **c**, Double hexamers assembled on bead-immobilized DNA with [α-^{32}P]ATP were used in CMG assembly reactions; the supernatants were analysed by scintillation counting. Error bars, s.e.m. **d**, Immunoblots of CMG assembly reactions carried out as in Extended Data Fig. 1a, except CDK was omitted, Sic1 was added, Sld2 and Sld3–Sld7 prephosphorylated with CDK were used, and the indicated nucleotide was added. Reactions were quenched 15 min after firing factor addition. **e**, As **d**, except reactions were carried out on soluble *ARS1* circles and analysed as in Fig. 2a. ATP was removed using a spin column after DDK phosphorylation.

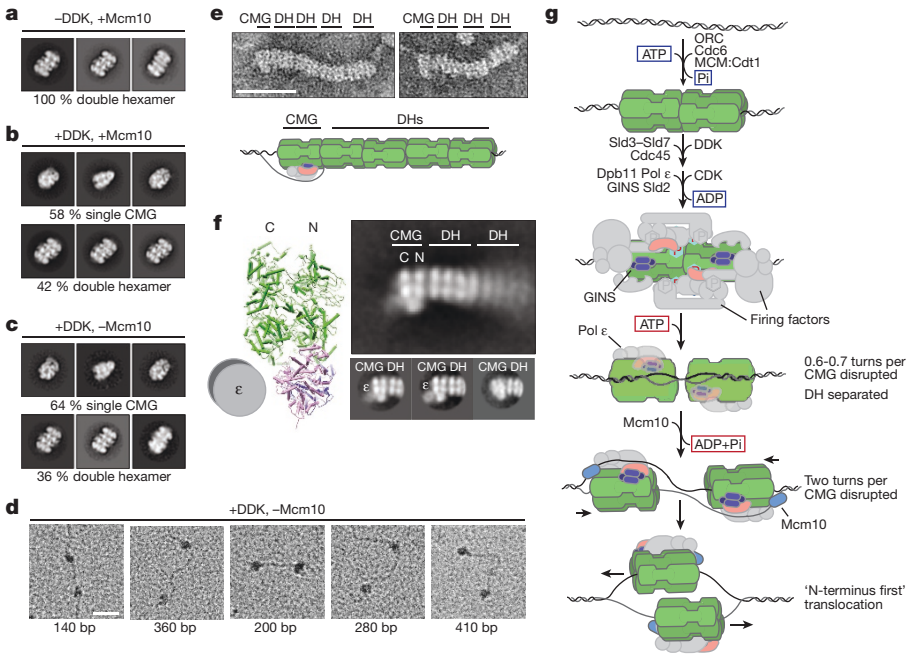

Figure 4 | Structural characterization of replicative helicase activation. **a**–**c**, Representative reference-free class averages of helicase activation reactions washed with high-salt buffer (buffer A + KCl). Double hexamer and CMG classes are shown. All particle classes are presented in Extended Data Fig. 4a. **d**, Helicase activation reactions lacking Mcm10 were washed with high-salt buffer and positively stained to visualize DNA. Examples of two CMG-sized particles co-localized with a single DNA fragment are shown. The approximate base-pair distance between particles is indicated. Scale bar, 50 nm. **e**, Examples of CMGs neighbouring double-hexamer trains (DH) in high-salt-washed reactions on roadblocked DNA. Scale bar, 50 nm. **f**, Annotated reference-free class average from 469 train ends. CMG structure (from Protein Data Bank code 3JC5) is included for reference. 2D classification of train tip particles into several classes (left to right, below) reveals doughnut-shaped polymerase ε density on a subset of CMGs (left and middle). **g**, Model of eukaryotic replicative helicase assembly and activation.

corresponds to a decrease in linking number of 1.3 (see Methods), indicating that each MCM hexamer untwists around 0.6–0.7 turns of DNA. Origin melting therefore proceeds via two distinct steps: untwisting of 0.6–0.7 turns per MCM hexamer during CMG assembly, and untwisting of approximately one further turn when CMG is activated by Mcm10.

ATP hydrolysis by MCM is required for double-hexamer formation[2,3], but nothing is known about the downstream roles of ATP in helicase activation. To investigate these roles, we first analysed nucleotide binding and release by the double hexamer. MCM that was loaded in the presence of [α-^{32}P]ATP and washed with high-salt buffer was bound to ADP with only background levels of ATP (Fig. 3a). Without further activation, ADP remained bound and did not exchange with unlabelled ADP, ATP or ATPγS over 30 min (Fig. 3b). To determine whether bound ADP is exchanged during helicase activation, MCM that had been primed with radiolabelled ADP as described above was used as a substrate for CMG assembly. Phosphorylation of MCM by DDK had little effect on the amount of bound ADP (Extended Data Fig. 3a), but ADP was released from the double hexamer into the supernatant of a full helicase activation reaction (Fig. 3c). ADP release was reduced in the absence of Sld2 or Sld3–Sld7, but not in the absence of Mcm10 (Fig. 3c), indicating that ADP release takes place during CMG assembly.

To examine the role of ATP binding and hydrolysis in CMG assembly, double hexamer was loaded onto bead-immobilized DNA, phosphorylated with DDK and washed to remove ATP and DDK. This DDK-phosphorylated double hexamer was then incubated with firing factors, including Sld2 and Sld3–Sld7 which had been phosphorylated by CDK and re-purified to remove ATP and CDK. After low-salt wash, Cdc45 and the GINS (as indicated by the Psf1 subunit) were recruited equally efficiently in a DDK-dependent manner in the presence or absence of nucleotide (Extended Data Fig. 3b, lane 3); however, challenge with high-salt wash showed that CMG assembly did not occur without added nucleotide (Fig. 3d, lanes 2 and 4). ATPγS supported stable CMG formation (Fig. 3d, lane 6), indicating that CMG assembly does not require ATP hydrolysis. To analyse the effect of nucleotide on DNA untwisting (Fig. 2), reactions were performed as in Fig. 3d, except soluble DNA circles were used as a template and ATP was removed from reactions using spin columns. Whereas no supercoiling occurred in the absence of ATP (Fig. 3e, lane 3), CMG assembly in reactions containing ATPγS and Mcm10 generated the same amount of supercoiling as in reactions containing ATP but lacking Mcm10 (Figs 2c, 3e (lane 5)). Together, these data show that CMG assembly and the initial untwisting of DNA are coupled to ADP release and ATP binding, whereas CMG activation by Mcm10 requires ATP hydrolysis. Mcm10 can stimulate ATP turnover by soluble MCM complex (Extended Data Fig. 3c), and may therefore trigger CMG activation by promoting ATP hydrolysis.

To characterize structural changes that occur during these processes, products assembled on bead-immobilized DNA were washed with high-salt buffer, released from beads by restriction enzyme digestion, and analysed by electron microscopy after negative staining. MCM-containing particles were only detected as double hexamers in reactions lacking DDK, Sld3–Sld7 or Dpb11 (Fig. 4a and Extended Data Fig. 4a, b). By contrast, in a complete reaction, nearly 60% of MCM-containing particles resembled discrete, single CMGs, indicating that approximately 40% of the input double hexamers had been activated (Fig. 4b and Extended Data Fig. 4a). In a reaction containing all firing factors except Mcm10, we observed the same proportion of discrete, single CMGs, after washing with either high- or low-salt buffer (Fig. 4c and Extended Data Figs 4a, c). Separation of the double hexamer therefore takes place during CMG assembly, before CMG is activated. We did not observe double CMGs in these reactions, and pairs of CMG-sized particles that co-localized on the same DNA molecule were separated by up to approximately 400 bp (Fig. 4d and Extended Data Fig. 4d), indicating that inactive CMGs move apart before activation.

CMG translocates in a 3′ to 5′ direction along the leading strand template[1], but its orientation at the fork is uncertain. The MCM hexamer is made up of two rings: one formed from the six C-terminal

AAA+ domains and one formed from the N-terminal domains. The hexamers in the double hexamer are linked by their N-terminal domains, and their C-terminal domains are on the outside of the hexamer. Therefore, if the C-terminal MCM ring is at the front of the helicase[13–15], then the two activated CMGs immediately move away from each other after initiation. If, however, the N-terminal ring is at the front[16], then the two hexamers must first pass each other during initiation. To investigate these possibilities, we used a 3-kb substrate containing covalent protein roadblocks at the end of each leading strand. We loaded an excess of double hexamers relative to DNA, activated a subset of these with the full set of firing factors, and analysed the products by electron microscopy after negative staining. Figure 4e and Extended Data Fig. 4e show images of multiple, adjacent double hexamers in 'trains' with a single CMG at one end. These were not seen if either Mcm10 or the roadblock was omitted (Extended Data Fig. 4f) indicating that active CMG pushes double hexamers, which are free to slide[9], and the roadblock prevents them from sliding off the DNA end. Comparing 2D averages of the ends of the trains with the structure of the CMG and its 2D projections (Fig. 4f and Supplementary Video 1) indicates that the CMG translocates with the N terminus of MCM in front of the helicase. In agreement with this orientation, a doughnut-shaped density characteristic of polymerase ε, which binds the C terminus of CMG[17,18], was observed in a subset of CMGs on the opposite side from the double hexamer (Fig. 4f and Supplementary Video 1).

Our results lead us to propose the model summarized in Fig. 4g. ADP formed during double-hexamer assembly remains stably bound to MCM—recent structural studies suggest that this probably occurs at only a subset of MCM active sites[11,12]. ADP is released in response to firing factors, and subsequent ATP binding by MCM triggers CMG assembly, during which double-hexamer separation takes place. The position of GINS in the CMG is sterically incompatible with the double hexamer[19], which suggests that these processes occur concomitantly. This step is also accompanied by the first stage of origin melting, when 0.6–0.7 helical turns are unwound per CMG. The earliest steps of origin melting by SV40 large T antigen[7] and *Escherichia coli* DnaA[20] are also triggered by ATP binding, suggesting that this is a conserved feature of replication initiation. The CMG is more than 10 nm in length, but at this stage contains less than 5 nm of ssDNA (6–7 bp fully stretched). Consequently, the lagging template strand cannot yet be entirely excluded from the MCM central channel. Full strand exclusion is required for CMGs to pass one another, indicating that the initial separation of hexamers must take place in the C-terminal direction. CMGs can separate by hundreds of base pairs *in vitro* without Mcm10 (Fig. 4d), but this movement may be restricted *in vivo* by nucleosomes. Moreover, Mcm10 can bind to the double hexamer before firing factor recruitment[21], which may facilitate immediate activation of CMG. Each active CMG constrains approximately two turns of untwisted DNA, which is long enough (around 15 nm) to be completely excluded from the central channel of MCM. Mcm10 binds avidly to ssDNA, and may therefore play a direct role in this exclusion process[22]. The order and timing of firing factor release is unknown, but Mcm10 has a subsequent role in elongation[8], suggesting that it may remain bound to the active helicase. Subsequent 'N terminus first' crossing of CMGs ensures that all origin DNA will be unwound, and may help to coordinate assembly of the two leading strand replisomes to ensure that this occurs only at origins. Furthermore, the requirement that two helicases can only pass one another when both are bound around ssDNA provides a fail-safe mechanism for bidirectional DNA replication, preventing CMGs from escaping the origin until both helicases are active. The ability of active CMG to push inactive double hexamers ahead of the fork (Fig. 4e, f) may be important for removal of unfired double hexamers from replicated DNA and to rescue stalled forks, but may also necessitate a pathway for double-hexamer removal before termination.

Online Content Methods, along with any additional Extended Data display items and Source Data, are available in the online version of the paper; references unique to these sections appear only in the online paper.

Received 19 May; accepted 29 December 2017.
Published online 28 February 2018.

1. Bell, S. P. & Labib, K. Chromosome duplication in *Saccharomyces cerevisiae*. *Genetics* **203,** 1027–1067 (2016).
2. Coster, G., Frigola, J., Beuron, F., Morris, E. P. & Diffley, J. F. X. Origin licensing requires ATP binding and hydrolysis by the MCM replicative helicase. *Mol. Cell* **55,** 666–677 (2014).
3. Kang, S., Warner, M. D. & Bell, S. P. Multiple functions for Mcm2–7 ATPase motifs during replication initiation. *Mol. Cell* **55,** 655–665 (2014).
4. Ilves, I., Petojevic, T., Pesavento, J. J. & Botchan, M. R. Activation of the Mcm2–7 helicase by association with Cdc45 and GINS proteins. *Mol. Cell* **37,** 247–258 (2010).
5. Georgescu, R. E. *et al.* Mechanism of asymmetric polymerase assembly at the eukaryotic replication fork. *Nat. Struct. Mol. Biol.* **21,** 664–670 (2014).
6. Yeeles, J. T., Deegan, T. D., Janska, A., Early, A. & Diffley, J. F. X. Regulated eukaryotic DNA replication origin firing with purified proteins. *Nature* **519,** 431–435 (2015).
7. Dean, F. B. & Hurwitz, J. Simian virus 40 large T antigen untwists DNA at the origin of DNA replication. *J. Biol. Chem.* **266,** 5062–5071 (1991).
8. Lõoke, M., Maloney, M. F. & Bell, S. P. Mcm10 regulates DNA replication elongation by stimulating the CMG replicative helicase. *Genes Dev.* **31,** 291–305 (2017).
9. Remus, D. *et al.* Concerted loading of Mcm2–7 double hexamers around DNA during DNA replication origin licensing. *Cell* **139,** 719–730 (2009).
10. Li, N. *et al.* Structure of the eukaryotic MCM complex at 3.8 Å. *Nature* **524,** 186–191 (2015).
11. Noguchi, Y. *et al.* Cryo-EM structure of Mcm2–7 double hexamer on DNA suggests a lagging-strand DNA extrusion model. *Proc. Natl Acad. Sci. USA* **114,** E9529–E9538 (2017).
12. Abid Ali, F. *et al.* Cryo-EM structure of a licensed DNA replication origin. *Nat. Commun.* **8,** 2241 (2017).
13. McGeoch, A. T., Trakselis, M. A., Laskey, R. A. & Bell, S. D. Organization of the archaeal MCM complex on DNA and implications for the helicase mechanism. *Nat. Struct. Mol. Biol.* **12,** 756–762 (2005).
14. Costa, A. *et al.* DNA binding polarity, dimerization, and ATPase ring remodeling in the CMG helicase of the eukaryotic replisome. *eLife* **3,** e03273 (2014).
15. Froelich, C. A., Kang, S., Epling, L. B., Bell, S. P. & Enemark, E. J. A conserved MCM single-stranded DNA binding element is essential for replication initiation. *eLife* **3,** e01993 (2014).
16. Georgescu, R. *et al.* Structure of eukaryotic CMG helicase at a replication fork and implications to replisome architecture and origin initiation. *Proc. Natl Acad. Sci. USA* **114,** E697–E706 (2017).
17. Sun, J. *et al.* The architecture of a eukaryotic replisome. *Nat. Struct. Mol. Biol.* **22,** 976–982 (2015).
18. Zhou, J. C. *et al.* CMG-Pol ε dynamics suggests a mechanism for the establishment of leading-strand synthesis in the eukaryotic replisome. *Proc. Natl Acad. Sci. USA* **114,** 4141–4146 (2017).
19. Abid Ali, F. *et al.* Cryo-EM structures of the eukaryotic replicative helicase bound to a translocation substrate. *Nat. Commun.* **7,** 10708 (2016).
20. Duderstadt, K. E., Chuang, K. & Berger, J. M. DNA stretching by bacterial initiators promotes replication origin opening. *Nature* **478,** 209–213 (2011).
21. Douglas, M. E. & Diffley, J. F. X. Recruitment of Mcm10 to sites of replication initiation requires direct binding to the minichromosome maintenance (MCM) complex. *J. Biol. Chem.* **291,** 5879–5888 (2016).
22. Robertson, P. D. *et al.* Domain architecture and biochemical characterization of vertebrate Mcm10. *J. Biol. Chem.* **283,** 3338–3348 (2008).

Supplementary Information is available in the online version of the paper.

Acknowledgements We thank K. Labib for anti-Psf1 antibody, G. Kelly (the Francis Crick Institute, Bioinformatics) for help with mathematical modelling, the Francis Crick Institute Fermentation Facility for cell production and L. Collinson, R. Carzaniga (the Francis Crick Institute, Electron Microscopy) and T. Pape (Electron Microscopy Centre, Imperial College) for electron microscopy support. This work was supported by the Francis Crick Institute, which receives its core funding from Cancer Research UK (FC001065 and FC001066), the UK Medical Research Council (FC001065 and FC001066), and the Wellcome Trust (FC001065 and FC001066). This work was also funded by a Wellcome Trust Senior Investigator Award (106252/Z/14/Z) and a European Research Council Advanced Grant (669424-CHROMOREP) to J.F.X.D.

Author Contributions All authors conceived the electron microscopy experiments; M.E.D. prepared the samples and F.A.A. performed the imaging. M.E.D. and J.F.X.D. conceived all other experiments, which were carried out by M.E.D. M.E.D. and J.F.X.D. wrote the paper with input from F.A.A. and A.C.

Author Information Reprints and permissions information is available at www.nature.com/reprints. The authors declare no competing financial interests. Readers are welcome to comment on the online version of the paper. Publisher's note: Springer Nature remains neutral with regard to jurisdictional claims in published maps and institutional affiliations. Correspondence and requests for materials should be addressed to J.F.X.D. (john.diffley@crick.ac.uk).

Reviewer Information *Nature* thanks A. Leschziner and the other anonymous reviewer(s) for their contribution to the peer review of this work.

METHODS

Protein purification. All proteins were purified as described[6].

DNA templates. Bead-immobilized linear and circular DNA templates were as described[6]. All plasmid-based assays used pBS/ARS1WTA, a 3.2-kb plasmid containing *ARS1*[23]. To assemble 616-bp *ARS1* circles, a 610-bp fragment around *ARS1* was PCR-amplified from this vector using oligonucleotides oMD171 and oMD172, which introduce recognition sites for EcoRI at both fragment ends. DNA (1.8 μg) was digested with 200 U EcoRI in 100 μl for 3 h at 37 °C, spin-column purified (Roche), and dephosphorylated with 5 U Antarctic phosphatase for 15 min at 37 °C. Phosphatase was inactivated at 70 °C for 5 min, and DNA ends were phosphorylated with PNK and [γ-^{32}P]ATP. PNK was heat-inactivated for 20 min at 65 °C, and the sample was desalted over a G50 spin column (GE) and ligated at a concentration of 180 ng/ml overnight at 10 °C with 20 U/ml T4 DNA ligase. The ligation reaction was concentrated 5–10 fold through a 10-kDa-cutoff spin filter (Millipore), ethanol precipitated and run on a 1× Tris-borate-EDTA (TBE) 1.5% agarose gel. DNA corresponding to supercoiled 616-bp circles was excised and electroeluted for 1 h in 0.1× TBE. The sample was ethanol precipitated and resuspended in 1× Tris-EDTA before use.

For the roadblocked DNA template used in Fig. 4e, f, a 2.8-kb fragment containing *ARS1* was amplified using oligonucleotides oMD203 and oMD204, which introduce a single recognition sequence for the methyltransferase HpaII on each end of the *ARS1* fragment. The PCR product was digested with XhoI and cloned into bluescript ks+ digested with XhoI and SmaI to make pMD142. pMD142 was used as a template for PCR with oMD215, which was biotinylated at the 5′ end, and oMD208. Methyltransferase HpaII was purified and coupled to this PCR product as described[24] and the coupled DNA product was immobilized on M280 streptavidin resin essentially as described[6], except resin was washed twice with 10 mM Tris pH 7.2, 1 mM EDTA and 1 M NaCl, twice with 10 mM Hepes pH 7.6, 1 mM EDTA, 1 M KOAc, and twice with 10 mM Hepes 7.6, 1 mM EDTA, and resuspended in half the starting resin volume with 10 mM Hepes 7.6, 1 mM EDTA.

Oligonucleotides. The sequences (5′ to 3′) of oligonucleotides used in this study are: oMD167, CGGAGGTGTGGAGAC; oMD171, TAGTAGGAATTCAAGCAGGTGGGACAGG; oMD172, TAGTAGGAATTCGCGAAAAGACGATAAATACAAG; oMD203, GGTGTATGCATGCTACTGTTTCTCGAGGTGTGAAAGTGGGGTCTCATCCTCAGCATCCGGTACCTCAGCGGTAGTTATAAGAAAGAGACCGAGTTAG; oMD204, GAGCCTGAATCCTCAGCATCCGGTACCTCAGCAAGAGTATTGGCGATGACGAAAC; oMD208, CAGGAAACAGCTATGACCATG; and oMD215, biotin–CGAAAAACCGTCTATCAGGGCGATG.

Assigning relative supercoiling states. To assign the relative supercoiling state of different 616-bp circle topoisomers, 2 fmol/μl 616-bp DNA circles were incubated at 65 °C for 30 min with 0.25 U/μl Nb.BsrDI enzyme, which specifically recognizes and nicks a single site on the circle. Nb.BsrDI was heat inactivated at 80 °C for 20 min, DNA extracted once with phenol:chloroform:isoamylalcohol (25:24:1) and ethanol precipitated. The DNA pellet was resuspended in 1× Tris-EDTA, and 3 fmol of the DNA was ligated in the presence of the ethidium bromide concentrations indicated at 10–12 °C overnight with 10 U/μl T4 DNA ligase (NEB). Ligated DNA was phenol:chloroform extracted, ethanol precipitated and the DNA pellet resuspended in 1× Tris-EDTA before analysis by electrophoresis. Final DNA circles are increasingly negatively supercoiled with increasing ethidium bromide during the ligation step. Topoisomers were therefore assigned relative to the ground state (α, the most prevalent topoisomer when ethidium bromide was omitted) by tracking the order in which bands peaked as the ethidium bromide concentration increased[25]. The nonlinear relationship between increased negative supercoiling and electrophoretic mobility (for example, compare mobility of topoisomers $\alpha-3$ and $\alpha-4$) has been seen previously[26] and may reflect extrusion of cruciform DNA, which is favoured as linking number decreases[27].

Unwinding assays. Plasmid DNA (25 fmol) or 616-bp DNA (5 fmol) was relaxed in 25 mM HEPES-KOH pH 7.6, 100 mM K-glutamate, 10 mM magnesium acetate, 0.02% NP-40-S, 5% glycerol, 2 mM DTT, 5 mM ATP (loading buffer), with 20 nM Topo I for 30 min at 30 °C. 5 nM ORC, 50 nM Cdc6 and 100 nM Mcm2–7:Cdt1 were added for 20 min at 30 °C, the reaction was supplemented with 50–100 nM DDK, and incubation continued for a further 30 min at 30 °C. Buffer was added to give a final concentration of 250 mM K-glutamate, 25 mM Hepes, 10 mM Mg-acetate, 0.02% NP-40-S, 8% glycerol, 400 μg/ml BSA, 5 mM ATP, 1 mM DTT and 25 nM Topo I (buffer CMG). A mix of firing factors was assembled immediately before use and added at time 0, to a final concentration of 50 nM Dpb11, 200 nM GINS complex, 50 nM Cdc45, 30 nM Pol ε, 20 nM Clb5–Cdc28 (CDK), 2.5 nM Mcm10, 30 nM Sld3–Sld7, 55 nM Sld2 (firing factor mix). After 40 min at 25 °C (for plasmid DNA) or 30 °C (for small circles), the reaction was quenched with 13 mM EDTA, 0.3% SDS, 0.1 mg/ml Proteinase K (Merck) (stop mix), and incubated at 42 °C for 20 min. Sample was extracted once with phenol:chloroform: isoamylalcohol (25:24:1), ethanol precipitated, and the DNA pellet resuspended in 1× Tris-EDTA for analysis.

Modified unwinding assays. The experiment in Fig. 2b was carried out as per unwinding assays, except no DDK was used, and no firing factor mix was added after dilution into buffer CMG. The experiment in Fig. 3e was carried out as per unwinding assays, with the following modifications: ATP concentration was reduced to 1 mM for the loading and DDK-phosphorylation steps. After phosphorylation, reactions were passed over a G50 spin column (GE healthcare) washed four times with 25 mM Hepes 7.6, 5 mM Mg-acetate, 10% (vol/vol) glycerol and 0.02% NP-40-S (buffer A) supplemented with 0.1 M K-glutamate. CDK was excluded from the firing factor mix; prephosphorylated Sld2 was used at a final concentration of 10–15 nM, and prephosphorylated Sld3–Sld7 at 10–20 nM. The prephosphorylation procedure is described below. Sic1 was added to a final concentration of 145 nM.

Gel electrophoresis. For plasmid-based unwinding assays, DNA was run on native 1.5% agarose Tris-acetate-EDTA (TAE) gels, at 1.5 V/cm for 16 h. Gels were stained with 0.5 μg/ml ethidium bromide for 1 h at room temperature, and destained with 1 mM Mg-sulfate for 1 h before imaging. For 616-bp circle unwinding assays, DNA was run on native 3.5% bis-polyacrylamide 1× TBE gels at 4.5 V/cm for 20 h.

Nucleotide-binding analysis. MCM loading reactions were carried out on 60 ng of immobilized 2.8-kb fragment of *ARS1*[6] in loading buffer with 500 μM ATP, 0.5 μCi/μl [α-^{32}P]ATP, 37.5 nM ORC, 50 nM Cdc6 and 100 nM Mcm2–7:Cdt1. After 30 min at 30 °C, beads were washed twice with buffer A supplemented with 0.5 M NaCl (buffer A + NaCl) and once with buffer A supplemented with 0.25 M K-glutamate and 2 mM $CaCl_2$ (buffer A + $CaCl_2$). DNA-bound complexes were released by cleavage with buffer A + $CaCl_2$ supplemented with 60 U/μl micrococcal nuclease (MNase) (NEB) for 5 min at 30 °C. Cleaved samples were spotted onto PEI-cellulose TLC plates (Camlab), which were developed in 0.6 M Na_2HPO_4–NaH_2PO_4 pH 3.5. For the nucleotide competition experiments in Fig. 3b, after the NaCl washes described above, DNA-bound complexes were washed once with buffer A + 0.1 M K-glutamate, and incubated at 30 °C for 15 or 30 min in buffer A + 0.1 M K-glutamate and 5 mM of the appropriate nucleotide. Samples were then washed once with buffer A + $CaCl_2$ and MNase-cleaved and analysed as above.

Recruitment assays. MCM-loading, DDK-phosphorylation and CMG-assembly steps were carried out as described in 'Unwinding assays', with the following modifications: each 20 μl CMG assembly reaction used approximately 60 ng linear DNA or 40 ng plasmid DNA immobilized on M-280 streptavidin magnetic beads[6] (Invitrogen). The concentration of ORC was increased to 37.5 nM. Supernatant was removed after DDK phosphorylation and DNA beads were resuspended in buffer CMG without Topo I. After CMG assembly and activation for 8 min, beads were washed twice with 200 μl buffer A with 0.3 M KCl (buffer A + KCl) or twice with buffer A with 0.25 M K-glutamate (buffer A + 0.25 M K-glutamate). After one further wash with 200 μl buffer A + $CaCl_2$, beads were resuspended in MNase, and cleaved for 5 min at 30 °C. Supernatant was supplemented with 1/3 volume of 4× SDS-loading buffer and heated at 95 °C for 3 min. Proteins were separated through 4–12% bis-Tris-polyacrylamide gels (Bio-Rad) and analysed by immunoblotting.

Modified recruitment assays. For the experiment in Fig. 2e, MCM loading and DDK phosphorylation were carried out in parallel on 16 fmol *ARS1* plasmid in solution or randomly biotinylated, and immobilized on Steptavidin M-280 resin (Invitrogen). Buffer CMG was added to four soluble reactions, two of which were immediately used to resuspend resin-immobilized reactions for samples 1 and 2. Firing factor mix without Mcm10 was added to all four samples at time 0. After 6 and 10 min, the two remaining soluble reactions were used to resuspend resin-immobilized reactions for samples 3 and 4, respectively. Eight minutes after addition of the soluble reaction to beads, resin was washed twice with 200 μl buffer A + KCl and once with 200 μl buffer A + $CaCl_2$, and DNA was cleaved with MNase for 5 min at 30 °C.

Recruitment assays with prephosphorylated Sld2 and Sld3–Sld7 involved the following modifications: the concentration of ATP was reduced to 1 mM for loading and DDK-phosphorylation steps, after which beads were washed three times with buffer A + 0.25 M K-glutamate. CDK was excluded from the firing factor mix and prephosphorylated Sld2 and Sld3–Sld7 were used at 10–15 nM and 10–20 nM, respectively. Sic1 was added to a final concentration of 145 nM.

For the electron microscopy assays in Fig. 4e, f, 120 ng linear, HpaII-coupled DNA immobilized on M-280 streptavidin magnetic beads was used per 20 μl CMG assembly reaction; Mcm2–7:Cdt1 was used at 200 nM during MCM loading.

Nucleotide-release analysis. Loading of MCM was carried out with [α-^{32}P]ATP as described in 'Nucleotide-binding analysis'. After 20 min at 30 °C, DDK was added to 100 nM. After a further 30 min at 30 °C, resin was washed twice with buffer A + NaCl and once with buffer A + 0.1 M K-glutamate, and resuspended in buffer CMG without Topo I. At time 0, firing factor mix (described in 'Unwinding assays')

was added. After 15 min at 30 °C, supernatant was collected, supplemented with 12.5 mM EDTA, mixed with 5 ml scintillation fluid and measured in a scintillation counter.

Protein prephosphorylation. Immediately before phosphorylation, Flag-tagged Sld3–Sld7 was diluted to 30 nM in 40 mM HEPES-KOH pH 7.6, 8% glycerol, 400 μg/ml BSA, 0.02% NP-40-S, 10 mM Mg-acetate, 2 mM DTT, 5 mM ATP with 310 mM K-glutamate (buffer PP + 310 mM K-glutamate). Sld2 was diluted to 120 nM in buffer PP + 235 mM K-glutamate. Clb5–Cdc28 was added to 10 nM, and reactions incubated for 8 min at 25 °C before addition of Sic1 to 220 nM. After 2 min incubation at 25 °C, Sld2 mix was diluted 4× in buffer A + 0.5 M KCl. Five microlitres magnetic anti-Flag M2 resin (Sigma), washed with buffer A + 0.5 M KCl, was added, and each sample incubated at 4 °C for 30 min with rotation. Resin was washed 5× with 300 μl buffer A + 0.5 M KCl (Sld3–Sld7) or buffer A + 0.35 M KCl (Sld2), and resuspended in 10 μl of the same buffer supplemented with 0.25 mg/ml Flag peptide. After shaking at 4 °C for 30 min, supernatant was collected, aliquoted and frozen in liquid nitrogen for storage.

Electron microscopy sample preparation. For positive and negative stain, CMG assembly was carried out as described in 'Recruitment assays'. Reactions were washed twice with 200 μl buffer A + KCl and once with 100 μl 25 mM Hepes, 5 mM Mg-acetate, 250 mM K-glutamate (buffer EM), and DNA-bound complexes were released from beads by restriction enzyme cleavage in 5–10 μl buffer EM supplemented with 0.1 U/μl MseI (NEB) for 10 min at 30 °C, giving rise to an average DNA fragment size of 1.5–2 kb. Negative-stain sample preparation was performed on 400-mesh copper grids (Agar Scientific) with floated carbon that had been freshly evaporated onto cleaved mica using a Q150TE coater (Quorom Technologies). Grids were glow-discharged for 30 s at 45 mA (Electron Microscopy Sciences). Three-microlitre drops of sample were applied to the grids and left to incubate for 1 min. Excess sample was blotted away and staining was performed on four separate 70-μl 2% uranyl formate drops by stirring for 5, 10, 15 or 20 s. Excess stain was blotted away and grids were stored before imaging. For positive stain, two-week-old carbon-coated 400-mesh copper grids (Agar Scientific) were glow-discharged for 10 s at 45 mA. 3 μl sample was applied and incubated for 30 s. Half the sample solution was blotted away before staining on a single 75-μl 2% uranyl acetate drop for 30 s. Stain was washed away by stirring the grid on four 75-μl ddH_2O drops for 5 s each before blotting the grid to dryness.

Electron microscopy data acquisition. Data collection of negative-stain grids was performed on a Tecnai LaB6 G^2 Spirit transmission electron microscope (FEI) operating at 120 keV (EM STP, The Francis Crick Institute). Micrographs were collected using a 2K × 2K GATAN Ultrascan 100 camera at a nominal magnification of 30,000 (3.45 Å pixel size) or 21,000 (4.92 Å pixel size, train classes) within a −0.5-to-2.5-μm defocus range. Analysis of positive stain grids was performed on a Tecnai G^2 F20 TWIN electron microscope operating at 200 keV (FEI; Electron Microscopy Centre, Imperial College London) equipped with a Falcon II direct electron detector (FEI). Micrographs were collected at a nominal magnification of 50,000 (2.05 Å pixel size) in a defocus range from −3 to −6 μm.

Electron microscopy single-particle analysis. Negative-stain particles were semi-automatically picked using EMAN2[28], version 2.07 and the rest of the image processing was performed using RELION[29] v1.4. Particles were extracted with a box size of 128 × 128 pixels (except the large train class in Fig. 4e, which was extracted with a box size of 250 × 250 pixels) from CTF-corrected (CTFFIND3[30]) micrographs and subjected to reference-free 2D classification with the –only_flip_ phases additional argument. Comparisons of 2D classes from different samples was performed using the multi-reference alignment function in IMAGIC[31].

Electron microscopy positive-stain image analysis. CMGs were distinguished from MCM double hexamers on positive-stain micrographs by measuring particle length parallel to the DNA axis using ImageJ. Examples where two particles were associated with the same fragment of DNA were analysed, and 84% of particles found to correspond to CMG (57/68). DNA fragments containing two CMG-sized particles are shown.

Potassium permanganate footprinting. CMG assembly and activation on small DNA circles were performed as in 'Unwinding assays' with the following modifications. The buffer for DNA relaxation and MCM loading was 25 mM Tris-Cl pH 7.2, 100 mM K-glutamate, 10 mM magnesium acetate, 0.02% NP-40-S, 5 mM ATP. After phosphorylation with DDK, buffer was added to give a final concentration of 250 mM K-glutamate, 25 mM Tris-Cl, 10 mM Mg-acetate, 0.02% NP-40-S, 400 μg/ml BSA, 5 mM ATP and 25 nM Topo I. After 10 min of CMG assembly at 30 °C, $KMnO_4$ was added to 3 mM for 4 min before the reaction was quenched with 1 M beta-mercaptoethanol (Sigma) and stop mix, and DNA processed as described in 'Unwinding assays'. The DNA pellet was resuspended in 48 μl 1× CutSmart buffer (NEB), digested with 40 U EcoRI-HF (NEB) for 20 min at 37 °C, extracted once with phenol:chloroform:isoamylalcohol (25:24:1), ethanol precipitated, and analysed by primer extension. Primer extension reactions contained ^{32}P end-labelled primer oMD167 and 70 U/ml Vent (exo-) DNA polymerase (NEB), and were carried out for 26 cycles. Reactions were quenched with stop mix, ethanol precipitated and separated on a denaturing 5% urea—bis—polyacrylamide gel.

DNA replication assay. For the experiment in Extended Data Fig. 1d, CMG assembly was carried out for 10 min as described in 'Recruitment assays', using a randomly biotinylated 5.6-kb *ARS1* plasmid immobilized on M280 steptavidin resin[6]. After CMG assembly in the presence or absence of Mcm10, resin was washed twice with buffer A + KCl (high-salt wash) or buffer A + 0.25 M K-glutamate (low-salt wash), and once with buffer A + 0.25 M K-glutamate. Beads were resuspended in 25 mM Hepes 7.6, 5 mM MgOAc, 0.02% NP-40S, 125 mM K-glutamate, 2 mM ATP, 1 mM DTT, 200 μM CTP, UTP, GTP, 40 μM each dNTP, 40 nM [α-^{32}P]dCTP (Perkin Elmer), 50 nM RPA, 30 nM Polymerase ε, 40 mM Polymerase α, 25 nM Topo I and 5 nM Mcm10 or Mcm10 buffer, and incubated for 45 min at 30 °C. Reactions were stopped and processed as described[6].

MCM ATPase assay. Mcm2–7 complex was diluted to 0.5 μM in buffer A + 0.5 M K-glutamate, containing 1 μM Mcm10. ATP was added to 100 μM, including 0.125 μCi/μl [α-^{32}P]ATP. After 30 min at 30 °C, EDTA was added to 15 mM and sample spotted onto PEI-cellulose TLC plates (Camlab), which were developed in 0.6 M Na_2HPO_4/NaH_2PO_4 pH 3.5.

Estimating linking number shift. When Mcm10 is omitted from an otherwise complete reaction, CMG is assembled on a fraction of circles, causing a shift in linking number by an unknown amount. If we denote Y_k as the abundance of a topoisomer k in the starting distribution of circles without CMG assembly (such as −DDK, lane 1 of Fig. 2c), when CMG is assembled, a proportion (a) of circles shift linking number by λ, such that for any k, a of k gets shifted to another state (k–λ), while the remaining (1–a) remains in state k. We can then model X_k, the abundance of k in the −Mcm10 reaction, as $X_k = Y_{k+\lambda}a + Y_k(1-a)$, where $Y_{k+\lambda}a$ is the fraction of topoisomer $k + \lambda$ that moves into state k in the −Mcm10 reaction, and $Y_k(1-a)$ is the amount of topoisomer k that remains in the −Mcm10 reaction after a fraction has moved to state k–λ. This can be rearranged to $(X_k - Y_k) = a(Y_{k+\lambda} - Y_k)$ which, given λ, can be solved by linear regression through the origin. Iterating through all possible values of λ on a grid, we choose the one for which residual mean square error was least. To enable fractional offsets to be calculated, we interpolated the original data using a cubic smoothing spline to give us estimated abundances at the resolution of tenths of an integer. A λ value of 1.3 at an efficiency (a) of 43% gave the best fit to the measured abundance of topoisomers in the −Mcm10 sample, with an R^2 value of 0.996. This is compared with shifts of 1.1, 1.2, 1.4 and 1.5, which gave R^2 values of 0.9716998, 0.9889401, 0.9888459 and 0.9653362 respectively.

Statistics and reproducibility. The experiments in Figs 1d, 2a, 2c, 3a, 3b, 3e and 4a–c were performed at least three times, while the experiments in Figs 1c, 2b, 3d and 4d, e were performed twice. The experiments in Extended Data Figs 1a, 2c–e and 4c were performed at least three times, while the experiments in Extended Data Figs 1b–d, 2b, 3b and 4d–f were performed twice. In Fig. 3c and Extended Data Fig. 3a, c, $n = 3$ independent experiments.

Data availability. The authors declare that the data supporting the findings of this study are available within the paper and its Supplementary Information files.

23. Marahrens, Y. & Stillman, B. A yeast chromosomal origin of DNA replication defined by multiple functional elements. *Science* **255,** 817–823 (1992).
24. Coster, G. & Diffley, J. F. X. Bidirectional eukaryotic DNA replication is established by quasi-symmetrical helicase loading. *Science* **357,** 314–318 (2017).
25. Shore, D. & Baldwin, R. L. Energetics of DNA twisting. II. Topoisomer analysis. *J. Mol. Biol.* **170,** 983–1007 (1983).
26. Zivanovic, Y., Goulet, I. & Prunell, A. Properties of supercoiled DNA in gel electrophoresis. The V-like dependence of mobility on topological constraint. DNA-matrix interactions. *J. Mol. Biol.* **192,** 645–660 (1986).
27. Hsieh, T. S. & Wang, J. C. Thermodynamic properties of superhelical DNAs. *Biochemistry* **14,** 527–535 (1975).
28. Tang, G. *et al.* EMAN2: an extensible image processing suite for electron microscopy. *J. Struct. Biol.* **157,** 38–46 (2007).
29. Scheres, S. H. RELION: implementation of a Bayesian approach to cryo-EM structure determination. *J. Struct. Biol.* **180,** 519–530 (2012).
30. Mindell, J. A. & Grigorieff, N. Accurate determination of local defocus and specimen tilt in electron microscopy. *J. Struct. Biol.* **142,** 334–347 (2003).
31. van Heel, M., Harauz, G., Orlova, E. V., Schmidt, R. & Schatz, M. A new generation of the IMAGIC image processing system. *J. Struct. Biol.* **116,** 17–24 (1996)

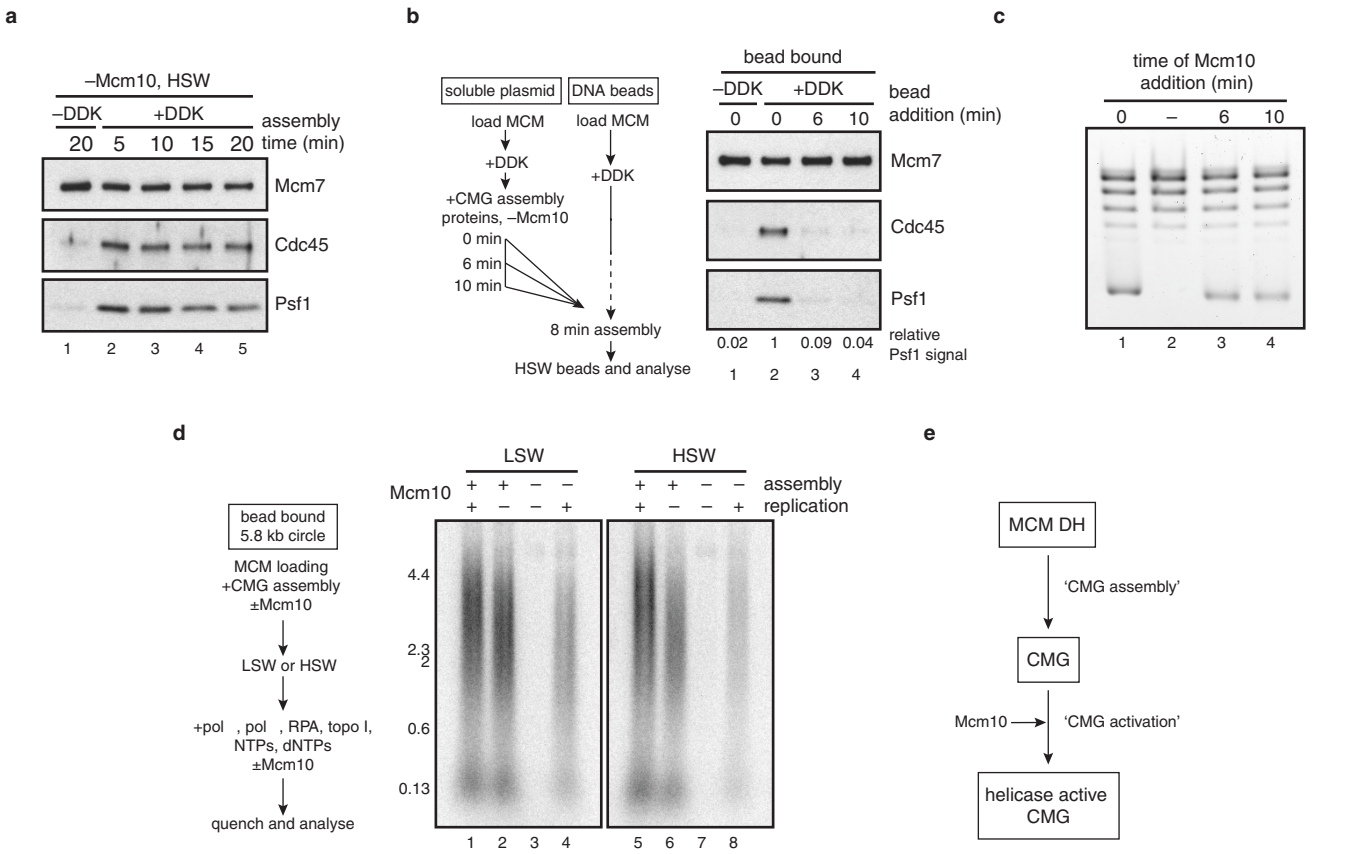

Extended Data Figure 1 | CMG assembly and activation are separable steps. a, To determine when CMG assembly saturates, reactions were carried out on bead-immobilized *ARS1* DNA and washed with high-salt buffer (HSW, buffer A + KCl) at the times indicated. The data show that no new CMG assembly takes place after 5 min. **b**, To confirm this, MCMs were loaded in parallel onto a bead-immobilized *ARS1* DNA fragment and a soluble *ARS1* plasmid, and phosphorylated with DDK. A firing factor mix, complete except for Mcm10, was added to the soluble reaction only, which was then added to the bead-immobilized MCMs at the times indicated after firing factor addition to the soluble reaction. After 8 min, beads were washed with high-salt buffer and bound proteins were analysed by immunoblotting. Psf1 signal relative to lane 2 is indicated. The experiment confirms that no CMG assembly takes place more than 5 min after firing factors have been added. **c**, To test whether Mcm10 can trigger DNA unwinding even after CMG assembly has finished, reactions were set up as in Fig. 1d, except Mcm10 was omitted until the times indicated after firing-factor addition. Mcm10 triggered robust unwinding, even when added more than 5 min after firing factors. Mcm10 can therefore activate preassembled CMG for DNA unwinding. **d**, To test whether Mcm10 can activate preassembled CMG for replication, CMG was assembled on an immobilized *ARS1* plasmid with or without Mcm10. Beads were washed with low- (Buffer A + 0.25 M K-glutamate, LSW) or high-salt buffer, and replication proteins with or without Mcm10 and cofactors, including radiolabelled dCTP, were added. Mcm10 enabled DNA replication even when CMG had been washed to remove excess firing factors. **e**, Schematic outlining the CMG assembly and CMG activation steps described here.

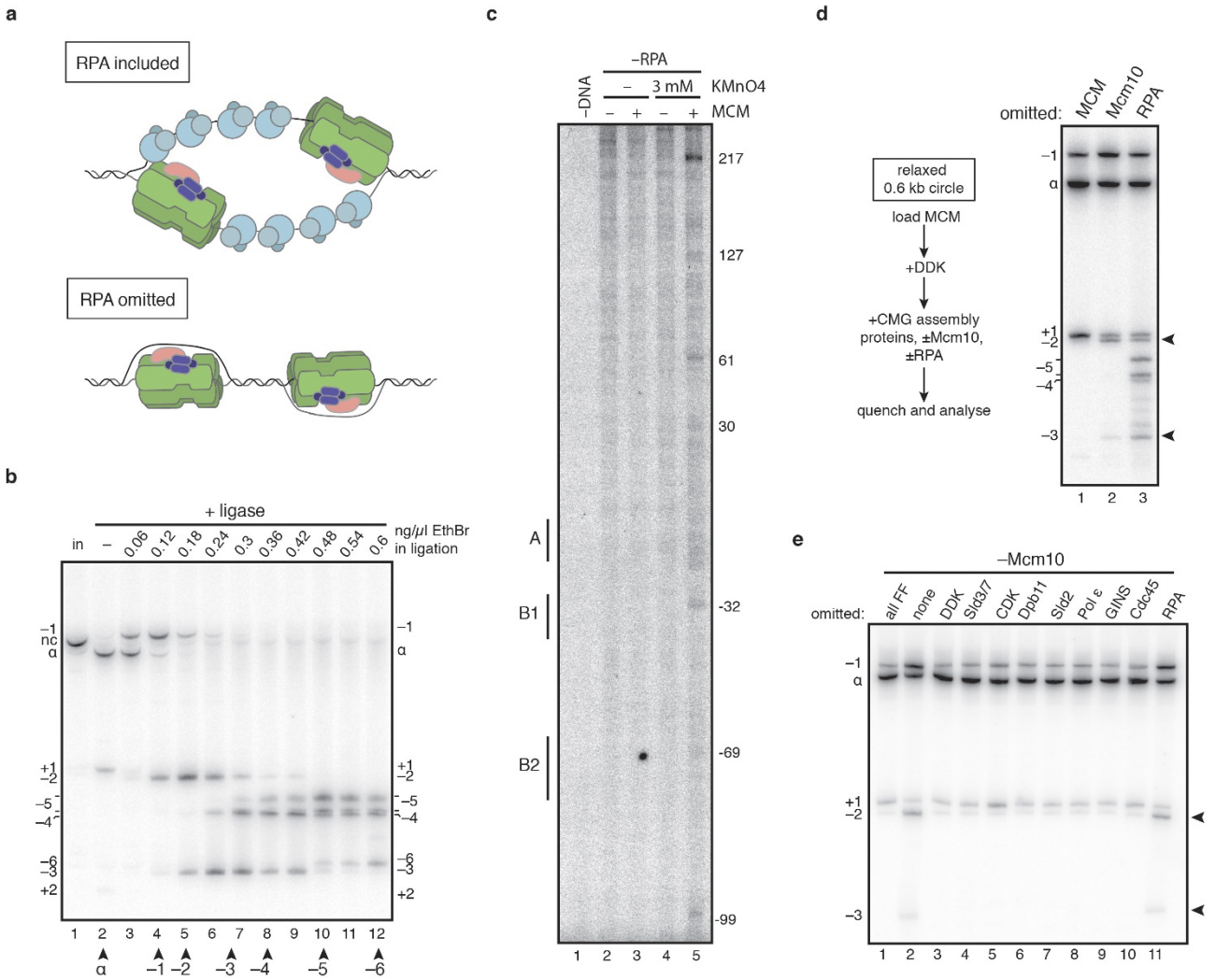

Extended Data Figure 2 | Characterization of DNA unwinding using small DNA circles. a, Models of DNA unwinding with or without RPA. **b**, To define the relative positions of different topoisomers of radiolabelled 616-bp DNA circles containing *ARS1* (used to analyse small changes in DNA supercoiling in the unwinding assay), nicked circles (nc, lane 1) were ligated closed in the indicated ethidium bromide (EthBr) concentrations. The supercoiling states of different bands of covalently closed DNA were determined relative to the ground state (α) by tracking the order in which bands peaked as ethidium bromide concentration increased and DNA was increasingly negatively supercoiled (see Methods for further details). Two bands peaked at the same position for α–5, and are likely to represent alternative configurations of the α–5 topoisomer. **c**, Primer extension reactions reading the T-rich strand of the ARS-consensus sequence (ACS) of *ARS1* were carried out using 616-bp *ARS1* DNA treated with potassium permanganate as indicated after CMG assembly in the absence of RPA. Reactions were separated on 5% sequencing gels, dried and analysed by autoradiography. Base pair numbering is relative to the 5′ end of the T-rich strand of the ACS. **d**, As Fig. 2c; lane 1 shows that MCM loading is required for all shifts in topoisomer distribution. Compared with other control samples, such as −DDK, topoisomer distribution was subtly different without MCM; this was not due to loading, which, as shown in Fig. 2b, does not affect topoisomer distribution. **e**, As Fig. 2a, except Mcm10 was omitted from all reactions. No proteins except Topo I were added to the reaction in lane 1 after MCM loading. There was no detectable change in supercoiling relative to when no firing factors (FF) were added (lane 1) when individual firing factors were omitted, suggesting that DNA untwisting in the absence of Mcm10 takes place during CMG assembly.

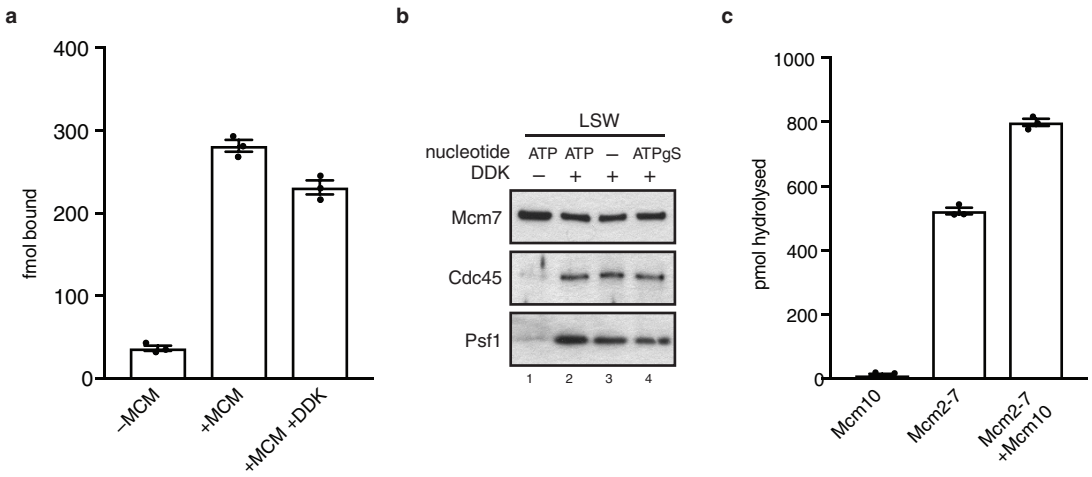

Extended Data Figure 3 | Analysis of nucleotide binding and turnover by MCM. a, Double hexamers assembled on bead-immobilized DNA using [α-^{32}P]ATP were treated with DDK as indicated, and analysed by scintillation counting. Error bars, s.e.m.. **b**, Immunoblots of CMG-assembly reactions carried out as in Fig. 3d and washed with low-salt buffer. **c**, ATPase assays using [α-^{32}P]ATP, single-MCM hexamers and Mcm10 as indicated were quantified after thin layer chromatography. Error bars, s.e.m.

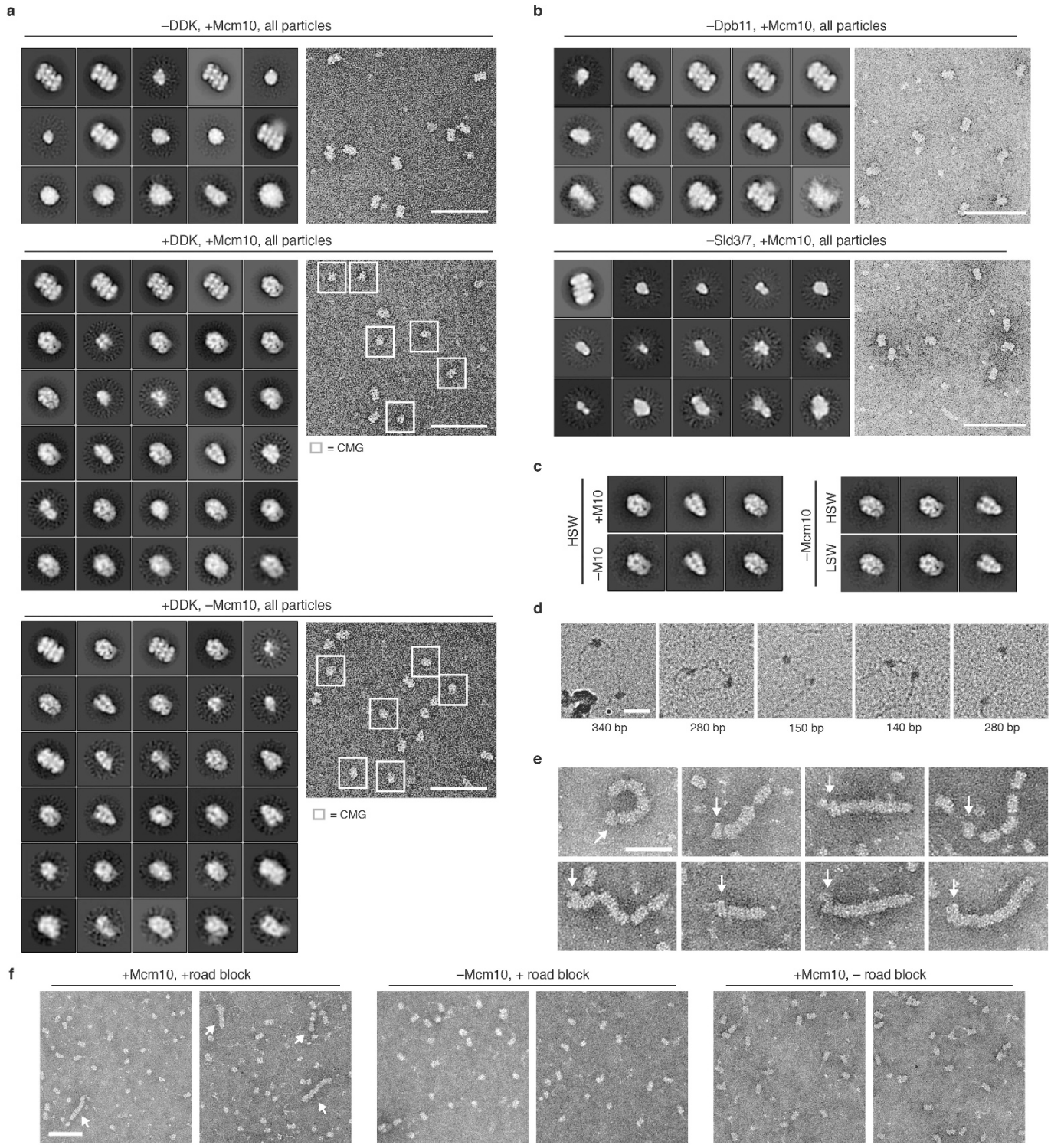

Extended Data Figure 4 | Characterization of replicative helicase activation using electron microscopy. a, Examples of micrographs and complete sets of reference-free class averages of the indicated helicase activation reactions, washed with high-salt buffer (buffer A + KCl). In −DDK, +Mcm10: 7,410 of 23,092 total particles were double hexamers. In +DDK, +Mcm10: 14,668 and 10,492 of 43,320 total particles were CMG and double hexamers, respectively. In +DDK, −Mcm10: 3,984 and 2,226 of 12,920 total particles were CMG and double hexamers, respectively. Classes are positioned with respect to the abundance of source particles, with the most abundant class in the top left-hand corner, and abundance decreasing from left to right and from top to bottom. **b**, As **a**, with representative source micrographs. 5,032 of 6,815 and 2,049 of 20,904 particles were double hexamers when Dpb11 or Sld3–Sld7 were omitted, respectively. Scale bar, 100 nm. **c**, Comparison of CMG formed in the indicated conditions. **d**, as Fig. 4d. **e**, As Fig. 4e. Arrows, position of CMG. **f**, Representative crops from micrographs of the indicated samples. Arrows, position of MCM trains. Trains were not observed when either Mcm10 or the protein roadblock was omitted. Scale bar, 100 nm.

nature research

Corresponding author(s): John Diffley

Initial submission ☐ Revised version ☐ Final submission ☒

Life Sciences Reporting Summary

Nature Research wishes to improve the reproducibility of the work that we publish. This form is intended for publication with all accepted life science papers and provides structure for consistency and transparency in reporting. Every life science submission will use this form; some list items might not apply to an individual manuscript, but all fields must be completed for clarity.

For further information on the points included in this form, see Reporting Life Sciences Research. For further information on Nature Research policies, including our data availability policy, see Authors & Referees and the Editorial Policy Checklist.

Experimental design

1. Sample size

Describe how sample size was determined.

No statistical methods were used to predetermine sample sizes. In the single-particle electron microscopy experiments 23,000 particles on average (300 micrographs) were collected for every data set. This data set size is sufficient 2-dimensional particle averaging with a resolution that reaches the limit imposed by negative stain electron microscopy.

2. Data exclusions

Describe any data exclusions.

For single-particle electron microscopy experiments, classes that were not recognised as containing the MCM helicase were excluded from the main figures (because they are not pertinent to our experiment). These excluded classes were instead shown in the supplementary figures.

3. Replication

Describe whether the experimental findings were reliably reproduced.

All experiments were performed a minimum of two times, as indicated in the 'Statistics and Reproducibility' section. For single-particle electron microscopy data, our findings were reliably reproduced upon repeating sample preparation with the same protein stocks. In vitro reconstituted replication initiation depends on multiple proteins that are purified independently. Variable efficiency of CMG formation was observed when using different protein preparations. However all of the conclusions from each electron microscopy experiment were confirmed (e.g. CMG formation alone, and not Mcm10 recruitment, causes splitting of the double hexamer).

4. Randomization

Describe how samples/organisms/participants were allocated into experimental groups.

For negative stain single-particle electron microscopy experiments, samples were allocated into different groups according to the experiment and the controls required to interpret the data. For example, to investigate whether Mcm10 had a role in the splitting of the MCM double hexamer, we compared samples with and without Mcm10. Further controls were designed (e.g, omission of DDK that prevents Cdc45 and GINS recruitment) to assess the quality of our assay and read-out. For the positive stain single-particle electron microscopy displayed in figure 4d, 123 micrographs from each of two datasets ±DDK were renamed with numerical values and the original identity of each numbered image was recorded. For analysis, images from the two datasets were mixed and assembled into a randomized stack using ImageJ.

5. Blinding

Describe whether the investigators were blinded to group allocation during data collection and/or analysis.

To analyse the positive stain dataset in figure 4d, particle lengths were measured from a stack containing a randomised mix of micrographs ±DDK (as described above). Group allocation only occured once all micrographs had been blindly scored.

Note: all studies involving animals and/or human research participants must disclose whether blinding and randomization were used.

6. Statistical parameters

For all figures and tables that use statistical methods, confirm that the following items are present in relevant figure legends (or in the Methods section if additional space is needed).

n/a	Confirmed
☐	☒ The exact sample size (*n*) for each experimental group/condition, given as a discrete number and unit of measurement (animals, litters, cultures, etc.)
☐	☒ A description of how samples were collected, noting whether measurements were taken from distinct samples or whether the same sample was measured repeatedly
☐	☒ A statement indicating how many times each experiment was replicated
☒	☐ The statistical test(s) used and whether they are one- or two-sided (note: only common tests should be described solely by name; more complex techniques should be described in the Methods section)
☒	☐ A description of any assumptions or corrections, such as an adjustment for multiple comparisons
☒	☐ The test results (e.g. *P* values) given as exact values whenever possible and with confidence intervals noted
☐	☒ A clear description of statistics including central tendency (e.g. median, mean) and variation (e.g. standard deviation, interquartile range)
☐	☒ Clearly defined error bars

See the web collection on statistics for biologists for further resources and guidance.

Software

Policy information about availability of computer code

7. Software

Describe the software used to analyze the data in this study.

For electron microscopy, Eman2 (v2.07) was used for micrograph inspection and particle picking, CTFFIND3 was used to CTF correct micrographs, Relion (v1.4 and v2.0) was used for all other subsequent image processing. IMAGIC was used for comparison of 2D class averages from different samples. ImageJ and Photoshop were used for all other image analysis. Prism7 and Numbers were used for handling of numerical data

For manuscripts utilizing custom algorithms or software that are central to the paper but not yet described in the published literature, software must be made available to editors and reviewers upon request. We strongly encourage code deposition in a community repository (e.g. GitHub). *Nature Methods* guidance for providing algorithms and software for publication provides further information on this topic.

Materials and reagents

Policy information about availability of materials

8. Materials availability

Indicate whether there are restrictions on availability of unique materials or if these materials are only available for distribution by a for-profit company.

no unique materials were used

9. Antibodies

Describe the antibodies used and how they were validated for use in the system under study (i.e. assay and species).

Mcm7 was detected with anti-Mcm7 (yN- 19, sc-6688, Santa Cruz). The Psf1 subunit of the GINS complex was detected with a sheep polyclonal antibody, a kind gift from Dr Karim Labib. Cdc45 was detected with a rabbit polyclonal antibody generated by the Diffley laboratory. All antibodies have been validated in multiple previous publications. See for example Yeeles et al, Nature 519, 431-435 (2015).

10. Eukaryotic cell lines

a. State the source of each eukaryotic cell line used.

No vertebrate cell lines were used

b. Describe the method of cell line authentication used.

No vertebrate cell lines were used

c. Report whether the cell lines were tested for mycoplasma contamination.

No vertebrate cell lines were used

d. If any of the cell lines used are listed in the database of commonly misidentified cell lines maintained by ICLAC, provide a scientific rationale for their use.

No vertebrate cell lines were used

Animals and human research participants

Policy information about studies involving animals; when reporting animal research, follow the ARRIVE guidelines

11. Description of research animals

Provide details on animals and/or animal-derived materials used in the study.	No research animals were used in this study

Policy information about studies involving human research participants

12. Description of human research participants

Describe the covariate-relevant population characteristics of the human research participants.	No human research participants were used in this study